



Decadal time gaps between mafic intrusion and silicic eruption obtained from chemical zoning patterns in olivine

Fidel Costa*, Sumit Chakraborty¹

Institut für Geologie, Mineralogie & Geophysik, Ruhr-Universität, Bochum. Bochum 44780, Germany

Received 5 May 2004; received in revised form 21 July 2004; accepted 17 August 2004

Available online 8 October 2004

Editor: B. Wood

Abstract

Intrusion of mafic magma in a silicic crustal reservoir has been reported in numerous studies of subduction-related volcanoes and is considered a main process for triggering explosive eruptions and for transferring geochemical signatures from the mantle to the crust. Here we determine the timescales between mafic–silicic encounters and eruption by exploiting the fact that during such interactions, magmas exchange crystals, and their mineral compositions will strive to equilibrate to the new environmental conditions. Specifically, we model the Fe–Mg zoning patterns of olivine found in the dacites, andesite, and quenched mafic inclusions of the Holocene zoned eruption of Volcán San Pedro (36°S, Chilean Andes). The San Pedro eruption is an example where mixing between silicic and mafic magmas produced intermediate compositions (e.g., andesite) at depth, in the magma reservoir. For modeling the compositional profiles, we took into account the anisotropy of Fe–Mg diffusion in olivine and also the effects of diffusion in multiple dimensions, aspects that have been largely neglected in previous works. The retrieved timescales for olivine–melt equilibration by diffusion display an array ranging from ~1 year for the most silica-rich dacite to ~50 years for the andesite. This array of timescales, rather than a single value, provides new insight into the details of mafic–silicic mixing at depth. They reveal processes that occur on a longer timescale than the days to weeks time gap for cases where the mafic intrusion triggered the eruption and they might be associated with the instances where seismic activity or significant inflation of the volcanic edifice was not immediately followed by eruption. On the other hand, the year to decade timescales that we report for producing magmas of intermediate composition (e.g. andesites) are much shorter than the 10^3 – 10^5 years inferred from U-series disequilibria data for igneous differentiation by closed-system fractionation to produce similar magma compositions at subduction zones.

© 2004 Elsevier B.V. All rights reserved.

Keywords: volcano; andesite; olivine; diffusion; eruption; timescales

* Corresponding author. Tel.: +49 234 322 4393; fax: +49 234 321 4433.

E-mail addresses: Fidel.Costa-Rodriguez@rub.de (F. Costa), Sumit.Chakraborty@rub.de (S. Chakraborty).

¹ Tel.: +49 234 322 4395; fax: +49 234 321 4433.

1. Introduction

Volcanoes and their eruptions are major agents that shape the landscape, climate, thermal and chemical

structure of the Earth, in addition to having triggered major biotic extinctions in the past. Arc volcanoes are particularly significant because they are the sites of hazardous explosive eruptions and play a key role in the formation of silicic continental crust [1–3]. Field work, geochemistry and petrography combined with experimental and modeling studies have established the main magmatic processes (e.g., partial melting of the mantle, crystal fractionation, magma mixing) that are involved in producing the different igneous rock series, and triggering mechanisms of explosive eruptions have been identified [4]. However, little is known about the duration or timescales on which such magmatic processes operate. Most of what we know about the timescales of magmatic processes comes from the study of the U-series disequilibria [5–10], which has established that about 10^3 – 10^5 years elapse between partial melting of the mantle and eruption. Closed system differentiation can produce high-silica magmas in subduction zones over similar timescales (10^3 – 10^5 years), although Sigmarsson [11] has shown that differentiation from basalts to intermediate magmas in Iceland happened within 10 years. However, the U-series disequilibria method cannot be applied reliably to open systems because the isotopic clock is disturbed. An alternative and complementary tool to determine the timescales of magmatic processes is kinetic modeling [12–28]. The power of the kinetic approach lies in that it relates timescales to specific processes, it can be used with rocks of any age, it is capable of accessing the short timescales of interest (days to hundreds of years), and can be applied to multiple grains making it possible to test reproducibility and obtain insight into the statistical distribution of the retrieved parameters. Diffusion modeling of crystals to retrieve timescales requires gradients in mineral composition which can be established during magma mixing (or mingling) and during interactions of the ascending magmas with the crust. In this regard, the occurrences of xenocrysts in many eruptive products should be regarded as an invaluable source of information to constrain the duration of open-system magmatic processes.

Here we introduce a methodology for determining the time elapsed between mafic–silicic magma interactions and eruption by modeling the concentration profiles of olivines from a suite of dacite to andesite lavas and quenched mafic inclusions of Volcán San

Pedro (36°S , Chilean Andes). We find a relation between eruption sequence or composition of the bulk rock and the retrieved timescales: some years for the dacites to decades for the andesite. This relation was only observed when we took care to avoid artifacts arising from the effects of Fe–Mg anisotropy of diffusion in olivine and from the use of compositional profiles acquired in one dimension to model three-dimensional crystals, and highlights the importance of using realistic modeling approaches to obtain reliable time information of magmatic processes. Previous works that have neglected these aspects of diffusion modeling have probably under- or overestimated the timescales of magmatic processes by as much as a factor of 6. The approach developed here could be applied to many other eruptions for which evidence of mafic–silicic interactions is clear [29–31].

2. The Holocene Volcán San Pedro zoned eruption

Volcán San Pedro is located in the southern volcanic zone of the Andes (36°S), and is the Holocene and most prominent volcanic edifice (3621 m asl) of the larger Quaternary Tatara–San Pedro Volcanic Complex [32–34]. Costa and Singer [35] distinguished between two periods of volcanic activity at San Pedro: an Older Holocene phase during which basaltic andesites and andesites produced a cone of $\sim 1 \text{ km}^3$, and a Younger Holocene eruption which is characterized by a chemically and mineralogically zoned sequence of silicic lavas ($\sim 1 \text{ km}^3$). This was followed by basaltic andesites which rebuilt the summit cone of Volcán San Pedro. This younger volcanic activity might have been triggered by the sector collapse of the southeastern flank of the older volcanic edifice, and started explosively, with the formation of a tephra fall dacitic deposit. We have concentrated on the products of the zoned eruption which comprises four units: (1) a biotite-hornblende-bearing dacite (unit Qcf1), (2) a dacite similar to the previous one (unit Qcf2) but containing minor proportions of quenched mafic inclusions (QMI) and gabbroic xenoliths [36], (3) a less silicic dacite (unit Qcf3) containing numerous QMI, two pyroxenes, and breakdown products of hornblende and biotite, and (4) a two-pyroxene andesite ($\sim 0.1 \text{ km}^3$; unit Qcf4). These lavas were erupted in sequence (from 1 to 4), and

record the downward tapping of a zoned magmatic reservoir. Using petrological and geochemical data, Costa and Singer [35] proposed that the zoned character of the eruption was due to incomplete mixing between the most silica-rich dacite and the basaltic andesites which rebuilt the summit cone. Moreover, the major and trace element zoning patterns of plagioclase phenocrysts of the most silica-rich dacite [32] indicate that the mafic–silicic interaction occurred at depth (~6 km, [37]), and not in the conduit. The main volume of individual plagioclase crystals of the dacite consists of normal zoning cycles that oscillate between An_{65-60} and An_{50-45} , before they progressively reach compositions of An_{40-35} at the rims. The high anorthite peaks are correlated with high Mg and Fe concentrations and can be attributed to the presence of thermal and compositional gradients induced by a hot mafic magma at the base of the silicic reservoir [35]. As we will show below, the conclusion that mixing occurred at depth is also reflected in the timescales that we obtain. Olivine crystals derived from a mafic magma are found within the glass matrix and in the quenched mafic inclusions that occur in the dacite and andesite lavas, and these should record the time span between initiation of magma mixing and eruption.

The chemical and mineralogical zonation of the silicic eruption is also reflected in intensive variables: the temperature (T) and oxygen fugacity (fO_2) of the most silica-rich dacite (Qcf1) has been estimated to be 850 ± 10 °C and $\sim 1.7 \times 10^{-12}$ bar (or close to the NNO+1 buffer [38]), respectively, from experimental constraints [37], and also the compositions of co-existing Fe–Ti oxides using both the Ghiorso and Sack [39] and the Andersen and Lindsley [40] Fe–Ti oxide solution models. The pre-eruptive temperature and fO_2 of the other flows were estimated using the compositions of co-existing Fe–Ti oxides [35]: 840–910 °C for Qcf2, 880–970 °C for Qcf3, 900–990 °C for the Qcf4, all at about NNO+1.

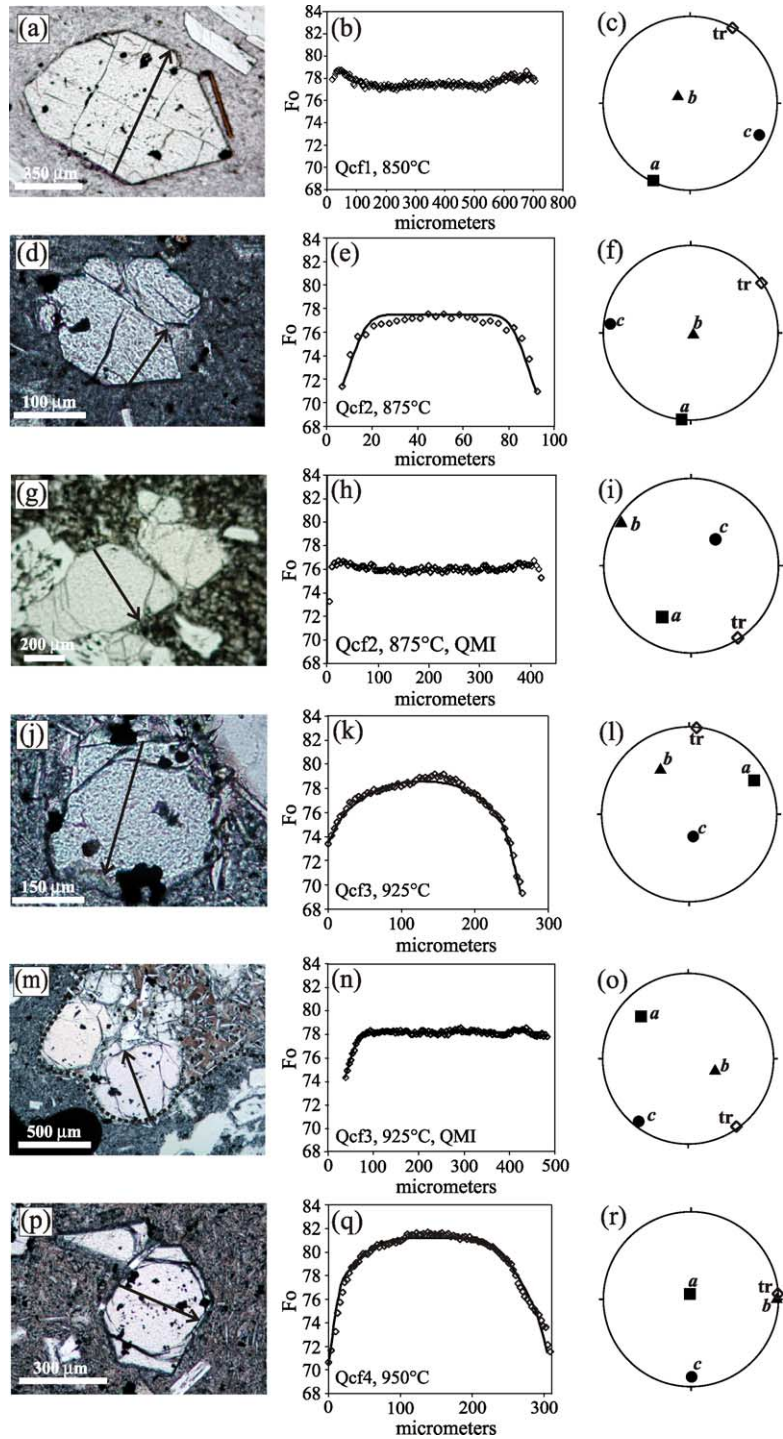
3. Olivine zoning profiles and textural observations

Rim to rim electron microprobe (Cameca SX-50) traverses with a spacing of 2–4 μm between analyses were performed across 32 olivine crystals ranging in size from ~50 to ~1200 μm . Most traverses were

done along the shortest dimension of the crystals, more or less parallel to a crystal face and through the center of the crystals. In the most silica-rich dacite (Qcf1) olivine is typically resorbed and surrounded by hornblende and orthopyroxene rims (~20 μm) except for some crystals which are euhedral (Fig. 1a). Olivine from the two other dacites (Qcf2 and Qcf3) and from the andesite (Qcf4) can be anhedral or euhedral but commonly lack reaction rims. Olivines from the most silica-rich dacite display nearly flat or normally zoned (decreasing values from core to rim) Fo content [$Fo = 100 * \text{Mg} / (\text{Mg} + \text{Fet})$ in mol; Fet=total iron], from Fo_{76} to Fo_{73} , with changes in composition only in the outermost 5–10 μm (Fig. 1a–c). Olivines from the two other dacites are normally zoned, from $Fo_{78 \pm 2}$ at the centers to Fo_{72-69} at the rims. The width of the zoned regions varies from ~20 μm in the Qcf2 (Fig. 1d–f) to ~150 μm in the most mafic dacite (Fig. 1j–l). Most olivines from the QMI show nearly constant compositions at $Fo_{78 \pm 2}$ with little or no zoning (Fig. 1g–i), except for those crystals with rims in contact with the silicic glass of the host which are normally zoned from $Fo_{78 \pm 2}$ at the centers to $Fo_{74 \pm 2}$ at the rims (Fig. 1m–o). Large olivine crystals in the andesite (Qcf4) show two distinct populations, one with a plateau composition at $Fo_{82 \pm 1}$, and another as that found in the dacite at $Fo_{78 \pm 1}$. Both types of olivines are normally zoned with rims of $Fo_{72 \pm 2}$ (Fig. 1p–r). The presence of two distinct maximum Fo contents (Fo_{78} and Fo_{82}) in the olivines from the andesite suggests that at least two mafic magmas were involved in the petrogenetic history of the V. San Pedro.

4. Model system

For proper interpretation of timescales obtained by modeling the concentration profiles of minerals, one needs to know the main igneous process that is responsible for the zoning patterns. In the present case, the petrological and geochemical observations of Costa and Singer [35] of the San Pedro zoned eruption indicate that the olivines found in the dacites and andesite originated from a mafic magma that forcefully intruded the silicic reservoir. Evidence of this mafic magma is found in the form of quenched mafic inclusions, although the fact that



more than one olivine population has been found in the andesite (see above) suggests that at least two mafic magmas intruded the silicic reservoir. Disaggregation of the inclusions dispersed the olivine crystals throughout the silicic reservoir and, thus, the olivine Fe–Mg zoning profiles are due to diffusion, and is a response of the olivines striving to equilibrate their compositions with the more silicic magma. This is supported by the fact that olivines inside the QMI have nearly constant compositions with little or no zoning (e.g., Fig. 1g–i), except where crystals from the QMI have rims in contact with the host lava (e.g., Fig. 1m–o). Thus, the timescales we obtain should record the time span between intrusion of the mafic magma and eruption. Costa and Singer [35] interpreted the zoned character of the eruption from dacite to andesite as due to partial hybridization of the most silicic dacite with a basaltic andesite and thus the timescales should also record the progressive creation of a zoned reservoir by magma mixing. As noted above, the magma mixing event occurred at depth and thus the timescales apply to deep-seated processes and not to those happening during eruption (e.g., magma mixing in the volcanic conduit).

5. Methodology of modeling

As in any diffusion model, one should clearly address the initial and boundary conditions at which diffusion took place. In addition, retrieval of timescales from modeling the concentration profiles in olivine crystals requires paying careful attention to various factors such as the compositional dependence and anisotropy of diffusion of Fe–Mg in olivines, the contribution of fluxes from more than one dimension and random sectioning effects. In the following, we

detail the modeling strategy that we have used and also the uncertainties.

5.1. Diffusion equation, initial and boundary conditions

The fact that Fe–Mg diffusion in olivine depends on the Fo content requires using an equation where the diffusion coefficient depends on the olivine composition. Thus, we have used the following expression of Fick's second law:

$$\frac{\partial C}{\partial t} = \frac{\partial}{\partial x} \left(D \frac{\partial C}{\partial x} \right) \quad (1)$$

where C is concentration, t is time, D is the diffusion coefficient, and x is distance, with the following initial and boundary conditions:

$$C = C_0, \quad t = 0 \quad (2)$$

$$C(r_1, r_2) = C_1, \quad t > 0 \quad (3)$$

where r_1 and r_2 are the coordinates corresponding to the rims of the crystal. Condition 2 expresses that we have used initial homogeneous compositions (C_0) either at $\text{Fo}_{78 \pm 1}$ or at $\text{Fo}_{82 \pm 1}$, corresponding to the maximum Fo values found in large olivines of all lavas (Table 1). If the olivines that entered the silicic lavas were already zoned, our calculations could overestimate the actual time that occurred between mixing and eruption. However, three observations suggest that using an initial flat Fo profile is realistic: (i) the zoning patterns of large olivines found in the coldest dacite are virtually flat or slightly reversed (Fig. 1a–c), (ii) olivines inside the QMI have little or no zoning (Fig. 1g–i), whereas crystals also from the QMI but with rims in contact with the host lava are zoned (Fig. 1m–o), and (iii) the length of the zoned portions of the crystals increases systematically from

Fig. 1. Representative photomicrographs of olivine crystals, diffusion models of the concentration profiles, and lower hemisphere projection of the orientation of the electron microprobe traverse (tr), relative to crystallographic axis (a , b and c) of olivine. Arrows on the photomicrographs show the position and direction of the compositional traverse. (a–c) Olivine found in the matrix glass of the coldest dacite shows flat or slightly reversed zoning in Fo content. (d–f) Olivine found in the matrix glass of a slightly hotter dacite shows normally zoned Fo composition. (g–i) Olivine inside a quenched mafic inclusions found in the same dacite as the previous crystal shows almost no Fo zoning. (j–l) Olivine crystal from the hottest dacite shows a pronounced zoned profile in Fo content. (m–o) Olivine crystal found in a quenched mafic inclusion of the same dacite as the previous crystal. Note that the rim of the olivine in contact with the host lava is zoned in contrast with the lack of zoning of the other rim which is in contact with the interior of the inclusion. Black dotted line in (m) marks the limit of the inclusion. (p–r) Olivine from the andesite shows pronounced Fo zoning. $\text{Fo} = 100 * \text{Mg}/(\text{Mg} + \text{Fe}_t)$ in mols, $\text{Fe}_t = \text{total iron}$. Open symbols in (b), (e), (h), (k), (n) and (q) are measured compositions and solid lines are best fit diffusion models to the data.

Table 1
Summary of calculated times and main attributes of the samples and olivine crystals

Sample	Crystal	<i>T</i> (°C)	SiO ₂ (wt.%) ^a	Initial Fo (mol%) ^b	ψ (°) ^c	1-D, non -oriented (years) ^d	1-D, oriented (years) ^e	2-D, oriented (years) ^f
Dacite (Qcf1)	1, 2, 4	850	65.8	78				<1 ^g
Dacite (Qcf2)	2in	875	64.5	78	17	12	48	21
	8	875	64.5	78	60	14	76	67
	9c	875	64.5	78	4	1.3	3	2
	9d	875	64.5	78	4	0.6	0.8	0.8
Dacite (Qcf3)	1in	925	63.6	78	7	2	9	9
	3in	925	63.6	78	28	3	15	9
	3b	925	63.6	77	58	6	33	26
	5	925	63.6	77	36	2	13	8
	6	925	63.6	82	60	21	127	91 (84, 5)
Andesite (Qcf4)	1in	950	61.4	78	50	12	65	52
	3c	950	61.4	83	5	10	59	44 (42, 2)
	7	950	61.4	78	68	0.5	2	2
	8	950	61.4	78	64	1.0	3	2
	9	950	61.4	78	60	1.1	5	5
	5	950	61.4	83	4	32	156	52 (49, 3)
	6	950	61.4	82	5	32	73	62 (57, 5)
	6c	950	61.4	83	47	13	28	28 (26, 2)
	6d	950	61.4	78	51	2	6	7

T=temperature.

In bold are the times that we consider more reliable because they were determined from crystals with small ψ (see text and Fig. 4). Crystal labels with 'in' at the end are those from mafic inclusions.

^a Of the bulk-rock, for detailed major and trace element analyses, see [35].

^b Initial composition used for modeling the crystal, Fo=100*Mg/(Mg+Fet) in mol, Fet=total iron.

^c Angle between the *c*-axis of the olivine and the thin section plane.

^d Calculated time only using diffusion in one dimension and assuming that the electron microprobe traverse is parallel to the *c*-axis of the olivine (e.g., Eq. (1)).

^e Calculated time in one dimension but taking into account the diffusion anisotropy of Fe–Mg.

^f Calculated time in two dimensions and taking into account the diffusion anisotropy of Fe–Mg. The numbers in parentheses are the times obtained from crystals that required two boundary conditions.

^g The short diffusion profiles (<10 μ m) displayed by olivines of this sample precluded detailed modeling, but we estimate a time of less than a year, because longer times would have produced a longer zoning profiles than we observe.

~20 μ m in the cold dacite to ~150 μ m for the hotter andesite, a trend that would not be present if olivines entered in the silicic magma with a significant amount of zoning.

The boundary condition is expressed by condition #3 above: we have used a single boundary composition (C_1) at the rims. This was the case for all olivine crystals with low Fo plateaus, but for olivines with high Fo (82 ± 1) plateaus, it was necessary to use two different compositions at the boundary. The significance of this observation is described below, but for these crystals we could retrieve two time estimates.

Finally, one should consider whether the olivine crystals were growing or dissolving because this would have an effect on the calculated timescales.

In the present case, there is a possibility that the olivine crystals were dissolving during their residence in the silicic magma. However, textural observations show that many olivines have rather euhedral crystal shapes (Fig. 1), so that although dissolution may have occurred it should not have substantially affected the timescales we have determined. In general, if the crystals were dissolving, the retrieved timescales from diffusion modeling would lead to underestimation of time, because the length of the diffusion profiles would have been shortened by dissolution.

5.2. Diffusion coefficient and anisotropy

For the diffusion coefficient of Fe–Mg in olivine, we have used the data of [41,42] which

describe D as a function of T , fO_2 , and Fo content:

$$D_c^{Fe-Mg} = 5.38 \cdot 10^3 \left(\frac{fO_2}{10^{-12}} \right)^{1/6} \cdot 10^{3 \left(\frac{86-Fo}{100} \right)} \times \exp \left[\frac{-226,000}{8.314T} \right] \quad (4)$$

where D_c is the diffusion coefficient of Fe–Mg parallel to [001] in $\mu m^2 s^{-1}$, T is in Kelvin, and fO_2 is in bars. This equation shows that D_c^{Fe-Mg} increases with decreasing Fo content and that it increases with increasing fO_2 . The exponent on the fO_2 is not yet very well characterized, but the available data [43,44] suggest that 1/6 is a good approximation. Moreover, Fe–Mg diffusion in olivine depends on the crystallographic direction, diffusion along [001] is about six times faster than along [100] or [010] [42,44], so that D_b^{Fe-Mg} and D_a^{Fe-Mg} were determined from D_c^{Fe-Mg} using the relationship $D_c^{Fe-Mg} \sim 6D_a^{Fe-Mg} \sim 6D_b^{Fe-Mg}$, independent of temperature [42]. Knowing D_c^{Fe-Mg} , D_a^{Fe-Mg} and D_b^{Fe-Mg} , it is possible to determine the diffusion coefficient along any analytical traverse using [45]:

$$D_{trav}^{Fe-Mg} = D_a^{Fe-Mg}(\cos\alpha)^2 + D_b^{Fe-Mg}(\cos\beta)^2 + D_c^{Fe-Mg}(\cos\gamma)^2 \quad (5)$$

where α , β and γ are the angles between the traverse and the a -, b - and c -axes of the olivine, respectively,

which we have determined by electron backscatter diffraction (EBSD; [46]). The orientations of the crystallographic axes and calculated profiles are shown as fits to the measured points in Fig. 1. Note that a diffusion model ignoring anisotropy or the effects of diffusion in more than one dimension (see below) would yield fits that are just as good, only the retrieved timescales would be incorrect (Fig. 2a; Table 1).

5.3. Diffusion in more than one dimension and the effect of using two-dimensional thin sections

To properly model the equilibration of a crystal with its surrounding melt, one should consider that

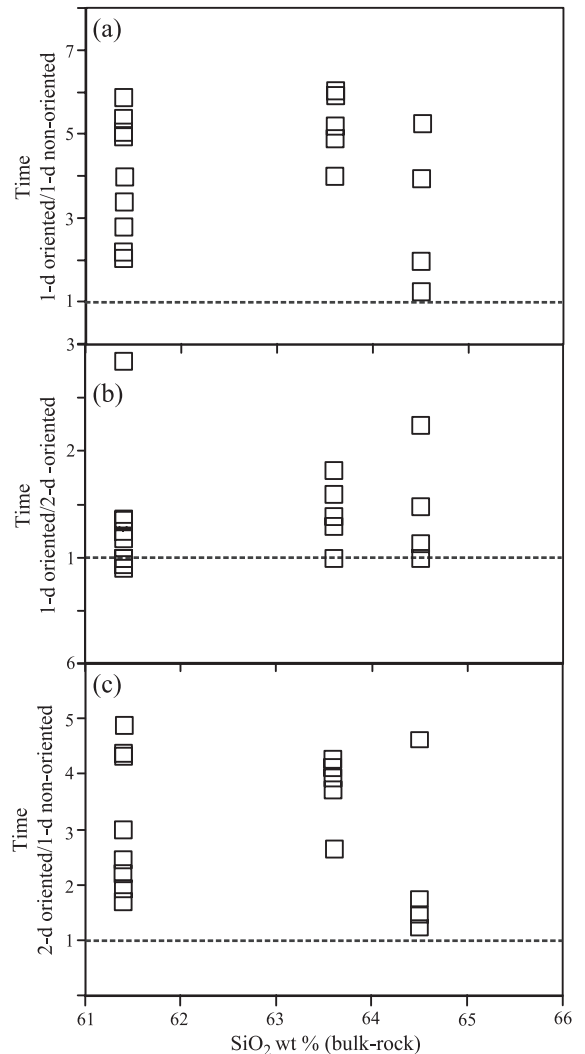


Fig. 2. Plots showing the effects on calculated times of taking into account the Fe–Mg diffusion anisotropy (1-D oriented) and of two dimensions (2-D oriented) compared to the times retrieved by a model that uses only a Fe–Mg diffusion coefficient along the c -axis (1-D non-oriented) for the different San Pedro samples (shown as the SiO_2 content of the bulk rock). The data are shown as the ratio of times obtained from different kinds of models. (a) Plot of the ratio between the times obtained by taking into account the Fe–Mg diffusion anisotropy (1-D oriented) and a model that uses diffusion coefficient along the c -axis (1-D non-oriented). It is apparent that neglecting anisotropy may result in underestimation of the calculated times by up to a factor of 6. (b) Plot of the ratio between the times obtained by taking into account the Fe–Mg diffusion anisotropy (1-D oriented) and a model that also considers the two-dimensional contribution to the diffusion (2-D oriented). The effect of modeling the crystals in two dimensions is to decrease the timescales, in this case up to a factor of 3. See also Fig. 3. (c) The overall effect on time determinations of the diffusion anisotropy and two dimensions (2-D oriented) compared to times retrieved by a model that uses only a Fe–Mg diffusion coefficient along the c -axis (1-D non-oriented).

flux of matter will occur in all three spatial dimensions (Fig. 3; F1, F2 and F3). As a first approximation (but see below), one can at least consider the flux from the two dimensions that are available for study using petrographic thin sections (F1 and F2) to assess the extent to which the two-dimensional effect will influence the calculated times (Fig. 3). This effect cannot be anticipated and depends on the amount of diffusion and the size and morphology of each particular crystal. Costa et al. [21] illustrated this problem using prismatic plagioclase crystals, and showed that not paying attention to the position of the compositional traverse

with respect to the morphology of the crystals can yield underestimation of timescales by factors larger than 3. The case of Fe–Mg diffusion in olivine has the same size and crystal morphology problems explained in [21] but with the added factor that Fe–Mg diffusion in olivine is quite anisotropic (see above) and thus the two-dimensional effect will be unavoidable in many instances.

An example of the importance of taking into account diffusion in two dimensions can be seen in Fig. 3 where we compare the results of modeling a hypothetical olivine crystal only in one dimension (e.g., by taking into account only the flux parallel to the direction of the measured data, F1) with those which incorporate the flux also from the direction perpendicular to the measured data (F2) and which resolve the problem of two dimensions (e.g., F1+F2).

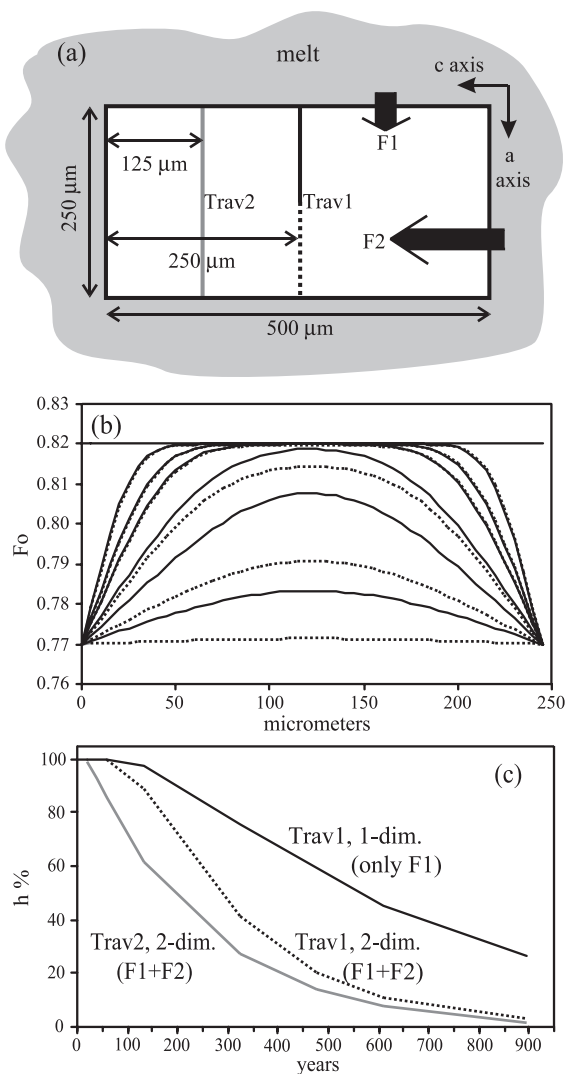


Fig. 3. Numerical calculations showing the effect of two-dimensional diffusion in modeling the Fe–Mg concentration in olivine. (a) Rectangular crystal ($500 \times 250 \mu\text{m}$) with the horizontal dimension parallel to the c -axis and the vertical dimension parallel to the a -axis. Also shown are the locations of two compositional traverses measured through the center of the crystal (Trav1, solid and dotted lines) and closer to the rim (Trav2, gray line). Note that in a real situation the crystal would exchange matter with the surrounding melt (shown as gray zone outside the crystal) in all three dimensions. In the figure, contributions of the fluxes from two of these dimensions are shown as large black arrows. F1 represents the flux from the direction parallel to the traverses and F2 is the flux from a direction perpendicular to them. Note that since diffusion parallel to the c -axis is six times larger than parallel to a or b , the contribution of the flux F2 is six times larger than that of F1. Not shown is the contribution of the flux from the direction perpendicular to the plane of the page (F3, but see Fig. 4). (b) Diffusion calculation for traverse 1 (Trav1) showing the time evolution of the concentration using a one-dimensional model which only takes into account the flux parallel to the traverse (F1, solid line) and a two-dimensional model that considers the contribution of the flux from the two directions (F1+F2, dotted line). The profiles are shown for the same period of time for both models. The evolution of the two-dimensional model is much faster even though the traverse is through the center and along the shortest dimension of the crystal. Note that a diffusion model ignoring anisotropy or the effects of diffusion in more than one dimension would yield as good fits to the natural data, only the retrieved timescales would be incorrect. (c) Plot of the time evolution of the concentration at the center of the crystal [$\% h = 100 \times (F_o - F_{o_{\text{equilibrium}}}) / (F_{o_{\text{initial}}} - F_{o_{\text{equilibrium}}})$] showing the effects of two dimensions and that of the position of the traverse (compare Trav1 with Trav2). Neglecting the flux from the horizontal direction (perpendicular to the traverse, Fig. 3a) can lead to overestimate of the time, in this specific example by a factor of 2–3.

The time evolution of the concentrations shows that even by measuring the olivine composition through the center of the crystal and along the shortest dimension, the timescales can be overestimated by a factor of 2 (Fig. 3c), and the effect is much larger for compositions that are not precisely measured through the center of the crystal (Fig. 3c). We note that the precise amount of neglected flux and thus the extent to which timescales will be overestimated depends on the size and position where the compositional data were acquired and thus it is typically different for each crystal. A lack of recognition of the two-dimensional effect in the San Pedro olivine crystals would have led to overestimation of time by up to a factor of ~ 3 (Fig. 2b). However, the combined effect of neglecting the Fe–Mg anisotropy of diffusion and that of two dimensions could have resulted in an underestimation of timescales by a factor of up to 5 (Fig. 2c).

The contribution of the flux from the third dimension is more difficult to evaluate but can be addressed by measuring the angle (ψ) between the section of the olivine plane and the c -axis of the olivine (Fig. 4; Table 1). Timescales obtained from modeling crystals with high ψ (e.g., $>45^\circ$) are unlikely to be correct, since the contribution of the flux from the third dimension was probably significant (because $D_c \gg D_a, D_b$) and unaccounted for in the two-dimensional models. We have therefore considered only the data obtained from crystals with $\psi < 45^\circ$ for deriving our geological inferences.

Using concentration profiles obtained from randomly sectioned three-dimensional crystals, as is the case when using conventional two-dimensional thin sections, could lead to incorrect estimation of timescales because the length and shape of the measured profiles could be affected. However, the effects can be recognized and minimized by avoiding the use of profiles that have dipping plateaus, and making sure that the maximum Fo plateau compositions of crystals of roughly the same size are the same [47]. Moreover, in a numerical experiment, Pan and Batiza [20] showed that only 20% of the times obtained from modeling Fe–Mg concentration profiles (using an isotropic diffusion coefficient) produced by randomly cutting a normally zoned sphere were shorter than the real time, and thus the effects of using two-dimensional thin sections should not compromise the retrieved timescales to a significant extent.

5.4. Uncertainties

As in most diffusion studies, the main uncertainty comes from the temperature estimation. A temperature uncertainty of 50°C varies the calculated times by a factor of 2–3 (for T between 950 and 850°C), and $f\text{O}_2$ uncertainty of 2 log units varies the times by a factor of ~ 2 . The temperature and $f\text{O}_2$ uncertainties for the present study are limited for the most evolved dacite (Qcf1) because both parameters are well constrained by Fe–Ti thermometry and experimental

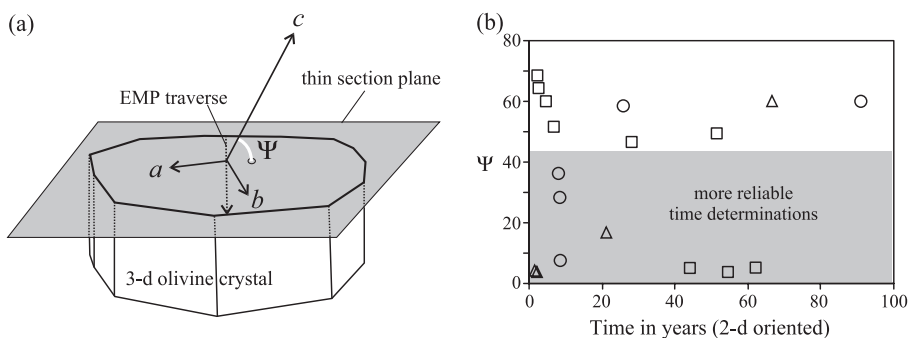


Fig. 4. (a) Schematic picture showing an olivine crystal (3-D olivine crystal), the plane of the thin section (gray) on which the composition of the olivine was measured with electron microprobe (EMP, dotted arrow), and the olivine crystallographic axes (arrows labeled a, b, c). ψ is the angle between the c -axis of the olivine and the thin section plane. (b) Plot of the angle (ψ) between the c -axis of the olivine and the plane of the thin section against calculated times considering the Fe–Mg diffusion anisotropy in olivine and two-dimensional effects (2-D oriented). Since diffusion parallel to the c -axis is a factor of 6 faster than along the a - or b -axis, timescales determined from crystals with $\psi < 45^\circ$ (gray area) are more reliable because the contribution of the flux from the third dimension is probably very small. Squares are time determination from olivines of the andesite, circles are those from dacite Qcf3, and triangles from dacite Qcf2.

work [37]. For the other samples, the temperature estimates by Fe–Ti thermometry should have an error of about 25 °C. Thus, the overall uncertainties in the worst case should be lower than a factor of 6, which still allows us to distinguish between timescales of months, decades or hundreds of years.

6. Results and discussion

We have modeled the zoning profiles of olivines with the diffusion coefficients and boundary conditions stated above and using a finite difference numerical solution to the diffusion equations. Example of fits to the natural data are shown in Fig. 1, and the calculated times are shown in Fig. 5 and Table 1. When all rock types and olivine crystals are considered, the retrieved timescales appear to vary widely, from about a year to ~90 years, with no apparent trend of calculated times as a function of eruption sequence or silica content (Fig. 4). However, considering only crystals with the more reliable low ψ values (Fig. 5; Table 1), a systematic trend between eruptive sequence

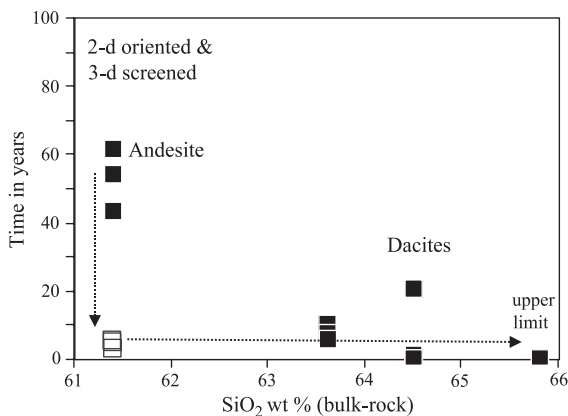


Fig. 5. Plot of the calculated times and the silica content or eruption sequence of the dacite and andesite lavas. These times were calculated considering the Fe–Mg diffusion anisotropy in olivine and two-dimensional effects (2-D oriented). The black squares are determinations obtained from olivines with a low ψ and are considered more reliable (3-D screened, see text and Fig. 4 for more details). Open squares denote times obtained for the last equilibration stage of the andesite. The data show that two mafic intrusions were involved in the petrogenetic history of V. San Pedro, one at about 50 years and the other at 2–5 years prior to eruption. This latter estimate is also found in the dacites. See text for more discussion.

and time emerges, and the range in calculated timescales decreases by half to vary between ~1 and 50 years. As noted above and shown in Table 1, we were able to calculate two times for crystals with high Fo (82 ± 1): the time for the last equilibration stage is between 3 and 5 years and coincides with the short timescales (2–7 years) obtained from crystals with lower Fo (78 ± 2). We interpret these data to imply that two mafic magmas intruded the silicic chamber at different times, one at 1–9 years, and the other at ~50 years before eruption. In this way, the two times obtained from the high Fo crystals reflect the physical process of transferring olivines from the mafic to the silicic magma: during an initial stage, the olivines remained enclosed in the mafic inclusions, but once the second mafic magma intruded (40–48 years later), the magma reservoir was disturbed anew, the inclusions were disaggregated and the olivines came into contact directly with the more silicic melt of the andesite. Such a process of disaggregation of mafic inclusions and transfer of crystals from mafic to silicic magmas has been described in other volcanic systems [29–31]. Irrespective of the details of the processes, these data imply that the timescales between intrusion of mafic magma and eruption are on the order of several years to some decades. Since the intrusion of mafic magma has played a main role in the petrogenetic history of the San Pedro magmatic system, these years to decades times also constrain the duration required for creating the zoned silicic reservoir and the intermediate andesite by magma mixing at depth. Complementary information for the residence time of these lavas comes from the study of a suite of gabbroic cumulate xenoliths found in the erupted products. Costa et al. [21] retrieved timescales varying from 30 to 150 years by modeling the trace element zoning patterns of plagioclase from the gabbroic xenoliths, which are consistent with our decadal time estimates.

The coexistence of the dacite and andesite at different temperatures within the magma reservoir places additional constraints on timescales from thermal considerations. We have used Eq. (9) of Snyder [48] to calculate the thermal homogenization time (T_h):

$$T_h = 0.26L \left(\frac{\rho C_p^2 \mu}{g \alpha \Delta T \lambda^2} \right)^{1/3}$$

where L =vertical thickness of the silicic magma, ρ =density, μ =effective viscosity, α =thermal expansion, λ =thermal conductivity, ΔT =temperature gradient, g =gravitational acceleration, C_p =effective heat capacity. All these values were calculated following [48]. In addition, we have used the following values [35,37]: 850 °C, 5.5 wt.% H₂O and 20 vol.% crystals for the dacite, and 950 °C, 2 wt.% H₂O and 30 vol.% for the andesite. Using $\Delta T=100$ °C and $L=1000$ m (because the total size of the eruption was 1 km³), we obtained $Th \sim 2$ years for the dacite and $Th \sim 3$ years for the andesite, which are approximations to having a magma reservoir completely filled with dacite or andesite. This is shorter than the maximum time of 50 years that we have obtained but very similar to the 2–5 years retrieved for the minimum timescales. While both the thermal and compositional modeling yield timescales on the order of years to decades, the correspondence of the thermal calculation to the lower end of the temporal spectrum obtained from compositional modeling may be caused by several factors, independently or in combination: (i) the simple boundary conditions of the thermal model may not be directly applicable to the San Pedro magmatic system where there is evidence of forceful injection of basaltic magma into the silicic magma chamber, rather

than simple underplating, and (ii) as we have noted above, there is evidence for injection of at least two mafic magmas. Therefore, the thermal model may reflect the timescale of relaxation of only one—the latest, of these pulses and this is also recorded in the shortest timescales obtained from the compositional record.

7. Implications for timescales of mixing, andesite formation, and eruption triggering

The new timescales of years to decades that we have obtained for intrusion of mafic magma, mixing, and eruption are substantially longer than those reported from petrological, numerical modeling and geophysical works on other volcanic systems, which are on the orders of hours to months (Table 2). For example, [25] estimated that mixing of dacite and basalt may occur in the matter of hours to days if it happens in the volcanic conduit, whereas numerical models [48–50] and seismological data for the 1991 Pinatubo eruption [51] suggests timescales of days to weeks between intrusion of basaltic magma into a silicic reservoir and eruption. Moreover, timescales ranging from days to 2 years have been reported from

Table 2
Summary of times related to mafic–silicic magma interactions or differentiation

References	Time (prior to eruption)	Magmatic system	Method	Process
[25]	hours to days	Saga–Futagoyama (Japan)	reaction coronas, plagioclase dissolution	basalt dacite mixing in conduit
[48–50]	days to weeks	various	numerical modeling	basaltic intrusion in silicic reservoir
[51]	days to weeks	Pinatubo (Philippines)	seismological data	basaltic intrusion in silicic reservoir
[14,17]	weeks to months	Unzen (Japan)	Fe–Ti oxide zoning	dacite–dacite mixing
[24]	days to 6 months	Ceboruco (Mexico)	Fe–Ti oxide zoning, plagioclase overgrowth	ryhodacite–dacite–mafic mixing
[18]	days to 2 years	Trident (Alaska)	Fe–Ti oxide and Fe–Mg olivine zoning	dacite–andesite mixing
[22]	10–1200 years	Montserrat (Lesser Antilles)	Sr and Ba plagioclase zoning	andesite remobilization by mafic intrusions
[23]	days to weeks	Montserrat (Lesser Antilles)	Fe–Ti oxide zoning	andesite remobilization by mafic intrusions
[5–10]	10 ³ –10 ⁵ years	Various subduction-zone volcanoes	Th–U, Ra–Th disequilibria	mafic to silicic closed system differentiation
[11]	10 years	Iceland	Pb–Ra disequilibria	mafic to intermediate closed system differentiation
This work	year to decades	San Pedro (Chile)	Fe–Mg olivine zoning	basaltic andesite–dacite mixing at depth

some volcanic systems for dacite–dacite, dacite–andesite, and rhyodacite–dacite–mafic magma mixing [14,17,18,24]. The differences of these timescales with the ones that we report can be explained by considering that: (i) the San Pedro eruption was induced by collapse of the eastern flank of the volcano [35] and, thus, intrusion of mafic magma did not necessarily trigger the eruption, (ii) magma mixing occurred at depth, in the reservoir [32,35], and thus longer timescales could be expected compared to mixing in the conduit, and (iii) in San Pedro, basaltic andesite and dacite magmas interacted extensively to produce the intermediate andesite whereas in other systems the two end-members were compositionally more similar [14,17,18,24]. It can also be possible that, in some cases, intermediate timescales (days to years) might reflect that the mixing process started at depth but continued in the conduit.

Our calculations show that immediate eruption following injection of mafic magma is not always the case and that petrological evidence of magma mixing should not be interpreted to have necessarily triggered a given eruption. Instead, the data that we report imply that to produce zoned silicic reservoirs and andesites by extensive mafic–silicic hybridization at depth, the time gap between intrusion of the mafic end-member and eruption has to be substantially longer than previously recognized, from years to decades. Moreover, these new time gaps between intrusion and eruption can be related to data obtained from seismic and deformation monitoring of active volcanoes. There have been several reports where seismic activity at depth was not immediately followed by eruption, but rather decades passed or eruption has yet to occur [52]. Similarly, monitoring of crustal deformation with tilt and interferometric synthetic aperture radar data has shown that subduction-related volcanoes can display periods of pre-eruptive inflation and post-eruptive deflation on the order of several years to decades, and the source (magma reservoir) has been constrained to be between 3 and 9 km deep [53,54]. These timescales and depths of magma reservoirs retrieved from deformation data are very similar to those obtained by kinetic and petrologic modeling for Volcán San Pedro. Thus, combination of real time monitoring of active volcanoes with detailed studies of erupted rocks could allow precursory activities to be related to specific magmatic processes.

On the other hand, compared to timescales of other magmatic processes that occur at depth and which produce intermediate (e.g. andesitic) compositions at subduction zones, our year to decade timescales are short. Andesite remobilization by intrusion of mafic magma appears to occur on timescales of a decade to 10^3 years [22], although it could be as short as days to weeks [23]. U-series disequilibria data suggest that to produce silica-rich magmas by closed-system crystal fractionation at subduction zones about 10^3 – 10^5 years are necessary [5–10], although in other tectonic settings (Iceland) it can be as short as 10 years [11]. Thus, each mode of producing magmas of intermediate composition (e.g., andesites) has a different and, perhaps, representative timescale: mixing in the conduit (hours to days), mixing at depth (years to decades), andesite remobilization (weeks to 10^3 years), and closed system fractionation (10^3 – 10^5 years). Therefore, determination of timescales from eruptive products may not only provide important clues to petrogenetic processes but also help to associate the time gaps between precursor activity (e.g., seismic and surface deformation data) and eruption to specific magmatic processes.

Acknowledgements

F.C. thanks M. Dungan and B. Singer for introducing him to the geology of San Pedro, and to C. Perring for help during field work. Comments and discussions with R. Dohmen and L. Coogan as well as reviews by C. Bacon, O. Sigmarsson, and S. Sparks are gratefully acknowledged. A grant from the Deutsche Forschungsgemeinschaft (DFG) under the SFB 526 program supported this work.

References

- [1] J. Gill, *Orogenic Andesites and Plate Tectonics*, Springer-Verlag, Berlin, 1981, p. 390.
- [2] P. Francis, J. Neuberg, R.S.J. Sparks, Causes and consequences of andesite volcanoes, *Philos. Trans. R. Soc. London Ser., A* 358 (2000) 1435–1729.
- [3] S.R., Taylor, S.M., MacLennan, *The Continental Crust: Its Composition and Evolution*, Blackwell Scientific Publication, London, 312 pp.

- [4] H. Sigurdsson (Ed.), *Encyclopedia of Volcanoes*, Academic Press, San Diego, USA, 2000, pp. 1417.
- [5] C. Hawkesworth, S. Blake, P. Evans, R. Hughes, R. Macdonald, L. Thomas, S. Turner, G. Zellmer, Time scales of crystal fractionation in magma chambers—integrating physical, isotopic and geochemical perspectives, *J. Petrol.* 41 (2000) 991–1006.
- [6] S. Turner, B. Bourdon, J. Gill, Insights into magma genesis at convergent margins from U-series isotopes, in: B. Bourdon, G.M. Henderson, C.C. Lundstrom, S.P. Turner (Eds.), *Uranium Series Geochemistry, Reviews in Mineralogy and Geochemistry* 52 (2003) 255–315.
- [7] M. Condomines, P.-J. Gauthier, O. Sigmarrsson, Timescales of magma chamber processes and dating of young volcanic rocks, in: B. Bourdon, G.M. Henderson, C.C. Lundstrom, S.P. Turner (Eds.), *Uranium Series Geochemistry, Reviews in Mineralogy and Geochemistry* 52 (2003) 125–174.
- [8] M.K. Reagan, K.W.W. Sims, J. Erich, R.B. Thomas, H. Cheng, R.L. Edwards, G. Layne, L. Ball, Time-scales of differentiation from mafic parents to rhyolite in North American Continental arcs, *J. Petrol.* 44 (2003) 1703–1726.
- [9] C. Hawkesworth, R. George, S. Turner, G. Zellmer, Time scales of magmatic processes, *Earth Planet. Sci. Lett.* 218 (2004) 1–16.
- [10] R. George, S. Turner, C. Hawkesworth, C.R. Bacon, C. Nye, P. Stelling, S. Dreher, Chemical versus temporal controls on the evolution of tholeiitic and calc-alkaline magmas at two volcanoes in the Alaska–Aleutian arc, *J. Petrol.* 45 (2004) 203–219.
- [11] O. Sigmarrsson, Short magma chamber residence time at an Icelandic volcano inferred from U-series disequilibria, *Nature* 382 (1996) 440–442.
- [12] S.C. Kohn, C.M.B. Henderson, R.A. Mason, Element zoning trends in olivine phenocrysts from a supposed primary high-magnesian andesite: an electron and ion-microprobe study, *Contrib. Mineral. Petrol.* 103 (1989) 242–252.
- [13] S.B. McKnight, C.R. Bacon, Olivine speedometry of multi-state magma mixing at Williams Crater, Crater Lake, Oregon, *Geol. Soc. Am. Abs. Progr.* 24 (1992) 69.
- [14] M. Nakamura, Continuous mixing of crystal mush and replenished magma in the on going Unzen eruption, *Geology* 23 (1995) 807–810.
- [15] M. Nakamura, Residence time and crystallization history of nickeliferous olivine phenocrysts from the northern Yatsugatake volcanoes, Central Japan: application of a growth and diffusion model in the system Mg–Fe–Ni, *J. Volcanol. Geotherm. Res.* 66 (1995) 81–100.
- [16] G.F. Zellmer, S. Blake, D. Vance, C. Hawkesworth, S. Turner, Plagioclase residence times at two island arc volcanoes (Kameni Islands, Santorini, and Soufriere, St. Vincent) determined by Sr diffusion systematics, *Contrib. Mineral. Petrol.* 136 (1999) 345–357.
- [17] D.Y. Venezky, M.J. Rutherford, Petrology and Fe–Ti oxide reequilibration of the 1991 Mount Unzen mixed magma, *J. Volcanol. Geotherm. Res.* 89 (1999) 213–230.
- [18] M.L. Coombs, J.C. Eichelberger, M.J. Rutherford, Magma storage and mixing conditions for the 1953–1974 eruptions of Southwest Trident volcano, Katmai National Park, Alaska, *Contrib. Mineral. Petrol.* 140 (2000) 99–118.
- [19] A. Klügel, Prolonged reactions between harzburgite xenoliths and silica-undersaturated melt: implications for dissolution and Fe–Mg interdiffusion rates of orthopyroxene, *Contrib. Mineral. Petrol.* 141 (2001) 1–14.
- [20] Y. Pan, R. Batiza, Mid-ocean ridge magma chamber processes: constraints from olivine zonation in lavas from the East Pacific Rise at 9°30' N and 10°30' N, *J. Geophys. Res.* 107 (2002) .
- [21] F. Costa, S. Chakraborty, R. Dohmen, Diffusion coupling between trace and major elements and a model for calculation of magma residence times using plagioclase, *Geochim. Cosmochim. Acta* 67 (2003) 2189–2200.
- [22] G.F. Zellmer, R.S.J. Sparks, C. Hawkesworth, M. Wiedenbeck, Magma emplacement and remobilization timescales beneath Montserrat: insights from Sr and Ba zonation in plagioclase phenocrysts, *J. Petrol.* 44 (2003) 1413–1431.
- [23] J.D. Devine, M.J. Rutherford, G.E. Norton, S.R. Young, Magma storage region processes inferred from geochemistry of Fe–Ti oxides in andesite magma, Soufriere Hills volcano, Montserrat, W.I., *J. Petrol.* 44 (2003) 1375–1400.
- [24] D.G. Chertkoff, J.E. Gardner, Nature and timing of magma interactions before, during, and after the caldera-forming eruption of Volcán Ceboruco, Mexico, *Contrib. Mineral. Petrol.* 146 (2004) 715–735.
- [25] H. Mashima, Time scale of magma mixing between basalt and dacite estimated for the Saga–Futagoyama volcanic rocks in northwest Kyushu, southwest Japan, *J. Volcanol. Geotherm. Res.* 131 (2004) 333–349.
- [26] C. Shaw, The temporal evolution of three magmatic systems in the West Eifel volcanic field, Germany, *J. Volcanol. Geotherm. Res.* 131 (2004) 213–240.
- [27] D.J. Morgan, S. Blake, N.W. Rogers, B. DeVivo, G. Rolandi, R. Macdonald, C.J. Hawkesworth, Timescales of crystal residence and magma chamber volume from modeling of diffusion profiles in phenocrysts: Vesuvius 1944, *Earth Planet. Sci. Lett.* 222 (2004) 933–946.
- [28] M. Coombs, J.E. Gardner, Reaction rim growth on olivine in silicic melts: implications for magma mixing, *Am. Mineral.* 89 (2004) 748–759.
- [29] T. Feeley, M. Dungan, Compositional and dynamic controls on mafic–silicic magma interactions at continental arc volcanoes: evidence from Cordón El Guadal, Tatara–San Pedro Complex, Chile, *J. Petrol.* 37 (1996) 1547–1577.
- [30] M. Clynne, A complex magma mixing origin for rocks erupted in 1915, Lassen Peak, California, *J. Petrol.* 40 (1999) 105–132.
- [31] Y. Ishizaki, Silicic–mafic magma interactions in a magma chamber beneath Tomuraushi volcano, Central Hokkaido, Japan, *Res. Geol. Spec. Issue* 20 (1999) 177–194.
- [32] B.S. Singer, M.A. Dungan, G.D. Layne, Textures and Sr, Ba, Mg, Fe, K, and Ti compositional profiles in volcanic plagioclase: clues to the dynamics of calc-alkaline magma chambers, *Am. Mineral.* 80 (1995) 776–798.
- [33] B.S. Singer, R.A. Thompson, M.A. Dungan, T.C. Feeley, S.T. Nelson, J.C. Pickens, L.L. Brown, A.W. Wulff, J.P. Davidson,

- J. Metzger, Volcanism and erosion during the past 930 k.y. at the Tatará–San Pedro complex, Chilean Andes, *Geol. Soc. Amer. Bull.* 109 (1997) 127–142.
- [34] M.A. Dungan, A. Wulff, R. Thompson, A refined eruptive stratigraphy for the Tatará–San Pedro Complex (36°S, Southern Volcanic Zone, Chilean Andes): reconstruction methodology and implications for magma evolution at long-lived arc volcanic centers, *J. Petrol.* 42 (2001) 555–626.
- [35] F. Costa, B.S. Singer, Evolution of Holocene dacite and compositionally zoned magma, Volcán San Pedro, Southern Volcanic Zone, Chile, *J. Petrol.* 43 (2002) 1571–1593.
- [36] F. Costa, M. Dungan, B.S. Singer, Hornblende- and phlogopite-bearing gabbroic xenoliths from Volcán San Pedro (36°S), Chilean Andes: evidence for melt and fluid migration and reactions in subduction related plutons, *J. Petrol.* 43 (2002) 219–241.
- [37] F. Costa, B. Scaillet, M. Pichavant, Petrologic and experimental constraints on the pre-eruption conditions of Holocene dacite from Volcán San Pedro (36°S, Chilean Andes) and the importance of sulfur in silicic subduction-related magmas, *J. Petrol.* 45 (2004) 855–881.
- [38] J.S. Heubner, M. Sato, The oxygen fugacity–temperature relationships of manganese nickel oxide buffers, *Am. Mineral.* 55 (1970) 934–956.
- [39] M. Ghiorsio, R. Sack, Fe–Ti oxide geothermometry: thermodynamic formulation and the estimation of intensive variables in silicic magmas, *Contrib. Mineral. Petrol.* 108 (1991) 485–510.
- [40] D.J. Andersen, D.H. Lindsley, Internally consistent solution models for Fe–Mg–Mn–Ti oxides: Fe–Ti oxides, *Am. Mineral.* 73 (1988) 714–726.
- [41] S. Chakraborty, Rates and mechanisms of Fe–Mg interdiffusion in olivine at 980 °C–1300 °C, *J. Geophys. Res.* 102 (1997) 12317–12331.
- [42] R. Dohmen, H.-W. Becker, S. Chakraborty, Point defect equilibration and diffusion in olivine at low temperatures ($T < 1000$ °C), *Eur. J. Mineral.* 15 (2003) 42.
- [43] D.K. Buening, P.R. Buseck, Fe–Mg lattice diffusion in olivine, *J. Geophys. Res.* 78 (1973) 6852–6862.
- [44] A. Nakamura, H. Schmalzried, On the nonstoichiometry and point defects of olivine, *Phys. Chem. Miner.* 10 (1983) 27–37.
- [45] J. Philibert, *Atom Movements, Diffusion and Mass Transport in Solids*, Les éditions de Physique, Les Ulis, France, 1991, p. 577.
- [46] D.J. Prior, A.P. Boyle, F. Brenker, M.C. Cheadle, A. Day, G. Lopez, L. Peruzzo, G.J. Potts, S. Reddy, R. Spiess, N.E. Timms, P. Trimby, J. Wheeler, L. Zetterström, The application of electron backscatter diffraction and orientation contrast imaging in the SEM to textural problems in rocks, *Am. Mineral.* 84 (1999) 1741–1759.
- [47] T.H. Pearce, The analysis of zoning in magmatic crystals with emphasis on olivine, *Contrib. Mineral. Petrol.* 86 (1984) 149–154.
- [48] D. Snyder, Thermal effects of the intrusion of basaltic magma into a more silicic magma chamber and implications for eruption triggering, *Earth Planet. Sci. Lett.* 175 (2000) 257–273.
- [49] R.S.J. Sparks, H. Sigurdsson, L. Wilson, Magma mixing: a mechanism for triggering acid explosive eruptions, *Nature* 267 (1977) 315–318.
- [50] A. Folch, J. Martí, The generation of overpressure in felsic magma chambers by replenishment, *Earth Planet. Sci. Lett.* 163 (1998) 301–314.
- [51] R.A. White, Precursory deep long-period earthquakes at Mount Pinatubo: spatio-temporal link to a basalt trigger, in: C.G. Newhall, R.S. Punongbayan (Eds.), *Fire and Mud: Eruptions and Lahars of Mount Pinatubo*, Philippines, Univ. Washington Press, Seattle, WA, 1996, pp. 307–327.
- [52] S.R. McNutt, Seismic monitoring, in: H. Sigurdsson (Ed.), *Encyclopedia of Volcanoes*, Academic Press, San Diego, USA, 2000, pp. 1095–1119.
- [53] J.J. Dvorak, D. Dzurisin, Volcano geodesy: the search for magma reservoirs and the formation of eruptive vents, *Rev. Geophys.* 35 (1997) 343–384.
- [54] D. Dzurisin, A comprehensive approach to monitoring volcano deformation as a window on eruption cycle, *Rev. Geophys.* 41 (2003).